remote sensing

MDPI

Article

Dynamic Evaluation of Agricultural Drought Hazard in Northeast China Based on Coupled Multi-Source Data

Kaiwei Li [1,2,3,4], Chunyi Wang [5], Guangzhi Rong [1], Sicheng Wei [1], Cong Liu [1], Yueting Yang [1], Bilige Sudu [1], Ying Guo [1], Qing Sun [5] and Jiquan Zhang [1,2,3,4,*]

1 School of Environment, Northeast Normal University, Changchun 130024, China
2 Jilin Province Science and Technology Innovation Center of Agro-Meteorological Disaster Risk Assessment and Prevention, Northeast Normal University, Changchun 130024, China
3 Key Laboratory for Vegetation Ecology, Ministry of Education, Changchun 130024, China
4 State Environmental Protection Key Laboratory of Wetland Ecology and Vegetation Restoration, Northeast Normal University, Changchun 130024, China
5 Chinese Academy of Meteorological Sciences, Beijing 100081, China
* Correspondence: zhangjq022@nenu.edu.cn; Tel.: +86-135-9608-6467

Abstract: As the climate warms, the impact of drought on plants has increased. We aimed to construct a comprehensive drought index (CDI), coupling soil-vegetation-atmosphere drought and heat conditions based on multi-source information, and to combine it with static and dynamic drought hazard evaluation models to analyze the spatial and temporal distribution characteristics of agricultural drought disasters and hazards during the growing season (May to September) in Northeast China (NEC). The results demonstrated that the CDI could combine the benefits of meteorology (standardized precipitation evapotranspiration index, SPEI), vegetation (vegetation health index, VHI), and soil (standardized soil moisture condition index, SMCI) indices. This was performed using a relative weighting method based on the remote sensing data of solar-induced chlorophyll fluorescence (SIF) to determine the weights of SPEI, VHI, and SMCI. The CDI for drought monitoring has the advantages of broad spatial range, long time range, and high accuracy, and can effectively reflect agricultural drought; the growing season in NEC showed a trend of becoming drier during 1982–2020. However, the trends of the drought index, the impact range of drought events, and the hazard of agricultural drought all turned around 2000. The drought hazard was highly significant ($p < 0.001$) and decreased from 2000 to 2020. The frequency of drought disasters was the highest, and the hazard was the greatest in May. The best level of climatic yield anomalies in maize were explained by drought hazard in August ($R^2 = 0.28$). In the center and western portions of the study area, farmland and grassland areas were where higher levels of hazard were most commonly seen. The dynamic hazard index is significantly correlated with climatic yield anomalies and can reflect the actual impact of drought on crop yield. The study results serve as a scientific foundation for drought risk assessment and management, agricultural planning, and the formulation of drought adaptation policies, as well as for ensuring food security in China.

Keywords: drought hazard; multi-source data; dynamic evaluation; drought and heat

Citation: Li, K.; Wang, C.; Rong, G.; Wei, S.; Liu, C.; Yang, Y.; Sudu, B.; Guo, Y.; Sun, Q.; Zhang, J. Dynamic Evaluation of Agricultural Drought Hazard in Northeast China Based on Coupled Multi-Source Data. *Remote Sens.* **2023**, *15*, 57. https://doi.org/10.3390/rs15010057

Academic Editor: Guido D'Urso

Received: 26 October 2022
Revised: 2 December 2022
Accepted: 20 December 2022
Published: 22 December 2022

1. Introduction

Drought is one of the most widespread, long-lasting, and daunting natural hazards globally, and is associated with heat waves, wildfires, and regional food security [1,2]. Extreme climatic events will become more frequent as a result of global warming, with droughts occurring frequently in conjunction with high temperatures. The decade from 2011 to 2020 was the warmest observed on record, and warming was greater at high latitudes than at low latitudes [3]. Northeast China (NEC), located in the middle and high latitudes, is one of the most vulnerable regions to climate change in China [4]. With a clear warm-dry trend, temperatures in the region have risen three times faster than the global average over the past century, and summer heat and drought events have increased in NEC in recent decades [4–7]. Drought is one of the most important factors driving grain output decline, accounting for 60.6% of the total economic loss in NEC [8]. NEC is a significant area in China for food production and ecological function, and crops in this area are significantly affected by extreme climatic events, particularly drought-heat and drought stress [4,9–12]. Therefore, in the context of global warming, research on the spatial and temporal distribution characteristics of drought disasters and hazards in NEC is extremely important to assess the effects of drought, prevent and mitigate agricultural disasters, and ensure ecological security.

Hazard is one of the key components of the disaster risk system, along with vulnerability, exposure, and capacity for disaster prevention and reduction [13]. The intensity and frequency (probability) of catastrophic activity play a major role in determining a hazard [14–16], and droughts that occur frequently or with high intensity may have serious adverse effects. Drought levels and their corresponding frequencies are commonly used to detect and quantify drought hazards [14,15,17]. Currently, the majority of studies on drought hazards have been conducted for static evaluation over a period of time, and there is a lack of dynamic evaluation of drought hazards for various years and different periods of the crop-growing season.

The Palmer drought severity index (PDSI), self-calibrating Palmer drought severity index (scPDSI), standardized precipitation index (SPI), standardized precipitation evapotranspiration index (SPEI), aridity index (AI), and others are commonly used meteorological station-based drought indices. These indices are effectively used to assess and monitor drought in various parts of the world [18–22]. Two of the most popular indicators for tracking meteorological droughts are the PDSI and the SPI. The PDSI is a drought index based on a water balance model that combines precipitation and evapotranspiration to capture the effects of global warming. The scPDSI has been improved to make it comparable across different climate zones [19]. In contrast to the SPI, which considers only precipitation, the SPEI considers both precipitation and potential evapotranspiration, capturing the impact of temperature rise on water demand [20]. However, these drought indices lack spatial continuity coverage and are insufficient for characterizing and monitoring the detailed spatial distribution of drought conditions, especially in areas where meteorological stations are sparse and unevenly distributed.

Remote sensing technologies enable the monitoring of soil moisture and vegetation conditions over large areas, extend the methods of drought monitoring, compensate for the disadvantages of spatial discontinuities in site-based drought indices, and capture temporal and spatial changes in surface states on a large scale [1]. The normalized difference vegetation index (NDVI) [23], vegetation condition index (VCI) [24], temperature condition index (TCI) [25], soil moisture condition index (SMCI) [26], and vegetation health index (VHI) based on vegetation and temperature [27], are commonly used for agricultural drought monitoring with good effects [28]. However, these indices have limitations. The vegetation index is an excellent visual indicator for plants after drought stress, but there is a lag in how quickly it responds to soil and meteorological drought. Other meteorological disasters, pests, and diseases can also cause a decline in the vegetation indices [1]. Additionally, the loss of land surface temperature (LST) product data caused by cloud pollution [29] may compromise the capacity to continue conducting efficient drought monitoring. Soil moisture is one of the most important indicators of agricultural droughts. However, the response of various crops to drought are not sufficiently reflected by soil moisture indicators, which only reflect the root environmental conditions for crop growth. The revisit cycle and consideration of only the surface layer (0–5 cm) in the satellite inversion of soil moisture restricts its ability to monitor drought. The data assimilation technique combines the benefits of remote sensing monitoring and model simulation, which can improve the temporal and spatial resolution of the observed data [30]. Agricultural drought is a complex process that involves several factors that may promote crop growth, such as meteorological conditions, crop biology, and soil properties. However, the above indicators generally ignore the physical mechanisms along the soil-plant-atmosphere continuum (SPAC) [31]. Therefore, a comprehensive drought index (CDI) based on multi-source information must be developed to monitor agricultural drought based on meteorological drought, soil drought, and vegetation response to drought to overcome the limitation of a single drought index to monitor the complex process of drought stress and to fully capture the various drought-influencing factors.

Because of its simple calculation, the CDI, which is created by integrating multi-source information such as meteorology, remote sensing, and data assimilation, and assigning values to different drought index weights using expert empirical weights [32], equal weights [33], correlation analysis [26], principal component analysis [34], and the entropy weighting method [31], is widely used for drought monitoring. In recent years, it has been suggested that monitoring plant photosynthesis from space using solar-induced chlorophyll fluorescence (SIF) is a promising technique. The SIF is regarded as an indicator of the functional state of plant photosynthesis. SIF has been demonstrated to be more representative of gross primary production (GPP) than vegetation index, with a higher sensitivity to environmental stress [35]. As a result, it has strong potential to detect vegetation responses to water deficit and heat stress. However, coarse resolution and short time scales hinder the application of SIF data. Researchers have used machine learning methods based on the OCO-2 Global SIF product (GOSIF) to obtain data at fine resolution (0.05°, 8 days) and longer time periods (2000–present) globally [36] to facilitate the study of SIF response to drought. However, it is still insufficient for drought and drought hazard analysis, which typically requires at least 30 years of data [37]. Therefore, this study proposes the use of the SIF data of a short time series (2000–2020), which is more sensitive to high temperatures and drought, as the dependent variable, and the meteorological drought index (SPEI), vegetation drought index (VHI), and soil drought index (SMCI) as independent variables. The relative weight method [38] was used to determine the weights of the independent variables to construct a comprehensive drought index for the long time series (1982–2020).

Therefore, NEC, which is sensitive to climate change, was used as the study area in this study. First, a comprehensive drought indicator CDI reflecting drought and its effects was built based on the SPAC theory by integrating data from multi-source information, such as meteorology, remote sensing, and reanalysis, and its applicability in the NEC region was confirmed. Second, the spatial and temporal distribution characteristics of drought were analyzed based on CDI. Finally, we constructed static and dynamic drought hazard assessment models to quantitatively assess drought hazard during the crop-growing season (May to September). The findings of this study are intended to provide a scientific basis for drought risk management, disaster prevention, and mitigation strategies in NEC.

2. Materials and Methods

2.1. Study Area

The study area is located in NEC, and includes a total of four provinces in Heilongjiang, Jilin, Liaoning, and northeastern Inner Mongolia. It has a complex topography and is surrounded by mountains on three sides (Figure 1a). The Northeast Plain is a vast region with rich black soil resources and deep fertile soils. It is one of the most significant grain-producing regions in China, with major crops including maize, rice, and soybean, and the growing season runs from May to September. NEC has a temperate continental monsoon climate with hot and rainy summers and cold, dry winters, with an average annual precipitation ranging from 400 to 1000 mm. From south to north, it shifts from a warm temperate zone to a cool temperate zone, and from east to west, from semi-humid to semi-arid regions. The complex topography and climatic conditions of NEC have shaped its diverse land cover types, of which 30.2%, 40.2%, and 19.4% are occupied by farmland, woodland, and grassland, respectively (Figure 1b).

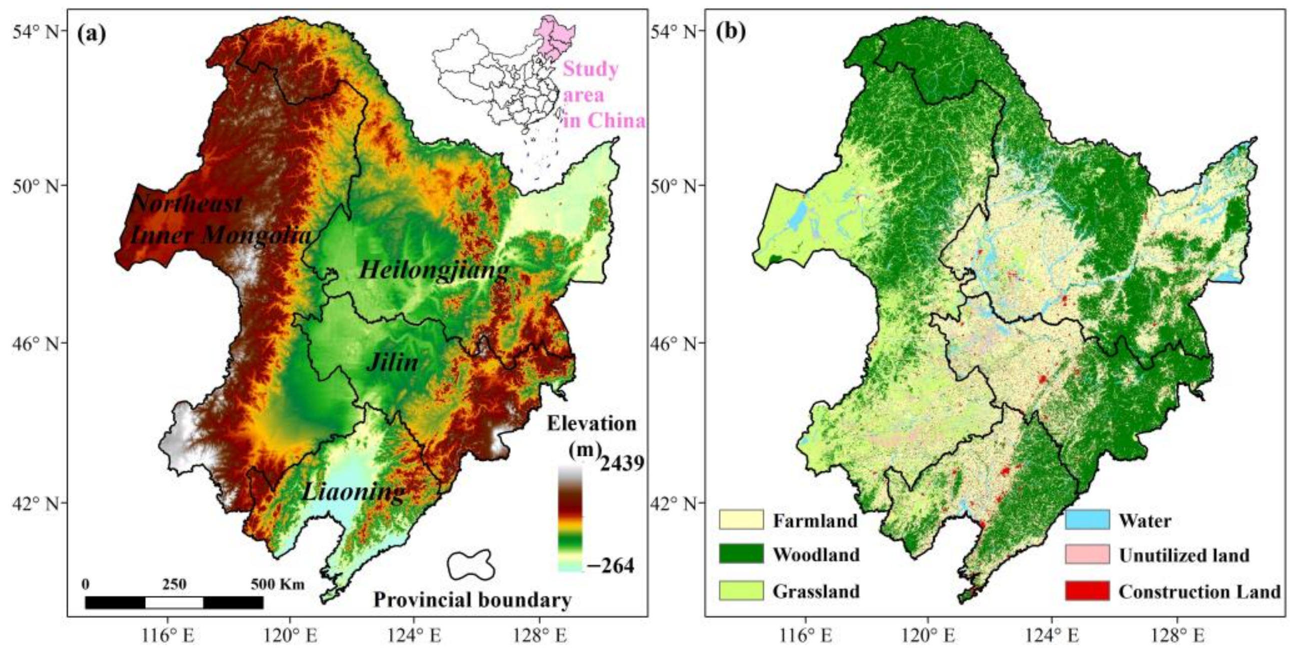

Figure 1. Location (**a**) and land use type (**b**) of the study area.

2.2. Data and Preprocessing

The primary data sources for this study were meteorology, remote sensing, soil, historical disasters, and yield data (Table 1). The SPEI was calculated using meteorological data from 113 weather stations in NEC, including daily precipitation, maximum and minimum temperatures, sunshine duration, wind speed, and average relative humidity. The VCI, TCI, and VHI were computed using the normalized difference vegetation index (NDVI) and the brightness temperatures (BT) extracted from remote sensing data. SMCI was calculated using root-zone soil moisture data obtained using data assimilation techniques based on satellite and reanalysis data. The SIF data were used to determine the weights of the atmospheric, vegetation and soil drought indices. The scPDSI, historical disaster data (area of drought-affected agricultural regions with total grain yield reduction exceeding 10% were used to evaluate the impact of agricultural drought) [39,40] and yield data were used to verify the validity of the CDI and hazard indices. All raster data were resampled to the same spatial and temporal resolution (4 ×4 km, monthly) using ArcGIS10.4 software.

Table 1. Data types and sources.

Data Type	Data Contents	Resolution	Time Span	Data Sources
Meteorological data	Daily precipitation, temperature, sunshine, wind speed and average relative humidity, etc.	113 weather stations in NEC	1960–2020	Meteorological Data Center of China Meteorological Administration (http://data.cma.cn/, accessed on 17 March 2022)
Remote sensing data	7-day NDVI, BT	4 × 4 km	1982–2020	Global Vegetation Health Products (https://www.star.nesdis.noaa.gov/smcd/emb/vci/VH/index.php, accessed on 17 March 2022)
	8-day SIF	0.05° × 0.05°	2000–2020	Global OCO-2 SIF data set (GOSIF) (https://globalecology.unh.edu/data/GOSIF.html, accessed on 17 March 2022)
	Land cover	1 × 1 km	2010	The Data Center for Resources and Environmental Sciences of the Chinese Academy of Sciences (RESDC) (http://www.resdc.cn, accessed on 17 March 2022)

Table 1. *Cont.*

Data Type	Data Contents	Resolution	Time Span	Data Sources
Soil data	Daily root-zone soil moisture	0.25° × 0.25°	1980–2020	The Global Land Evaporation Amsterdam Model (GLEAM v3.6a) datasets (https://www.gleam.eu/, accessed on 17 March 2022)
Historical disaster data	Drought-affected agricultural areas	Provinces in NEC	1986–2015	The Crop and Disaster Databases of the Ministry of Agriculture of the People's Republic of China (http://www.zzys.moa.gov.cn/, accessed on 17 March 2022)
Yield data	Maize yield and area	Provinces in NEC	1980–2020	National Bureau of Statistics of China (https://data.stats.gov.cn/, accessed on 17 March 2022)
Other data	scPDSI	4 × 4 km	1960–2020	Terra climate data sets (http://www.climatologylab.org, accessed on 17 March 2022)

2.3. Methods

2.3.1. Comprehensive Drought Index (CDI)

The soil-plant-atmosphere continuum (SPAC) is a unified, dynamic, and continuous system with mutual feedback [31], and there are response relationships among different types of drought indicators, such as meteorology, soil, and vegetation data. Therefore, we first selected the SPEI, considering the effects of precipitation and temperature to represent the meteorological index; SMCI, considering root-zone soil moisture to represent the soil index; and VHI, considering the vegetation condition (VCI) and temperature condition (TCI) to represent the vegetation index to construct the CDI. Second, the SIF data of the short time series (2000–2020), which is more sensitive to high temperatures and drought, were used as dependent variables, and the SPEI, VHI, and SMCI after standardization were used as independent variables. The relative weights analysis (rwa, https://github.com/martinctc/rwa (accessed on 17 March 2022)) [38] was used to determine the weights of the independent variables to construct the CDI for the long time series (1982–2020). Figure 2 shows the framework for CDI based on the SPAC.

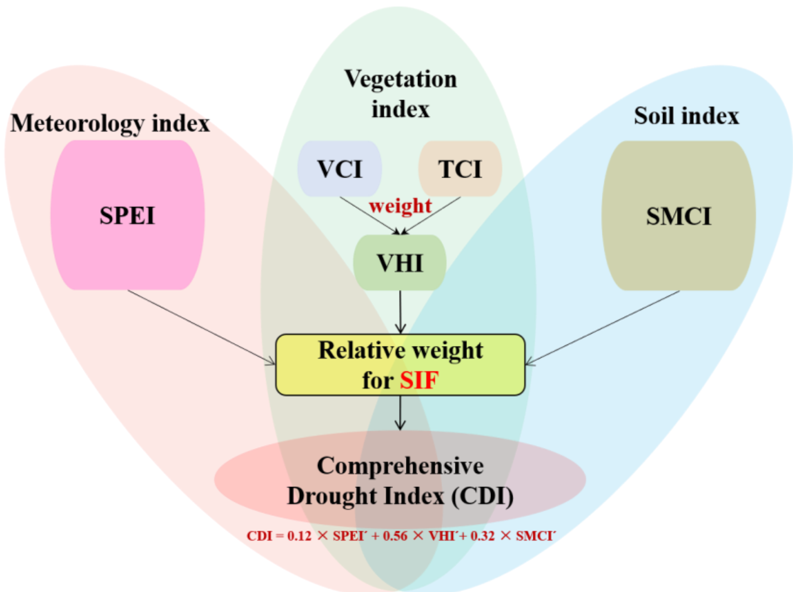

Figure 2. Framework for comprehensive drought index based on the soil-plant-atmosphere continuum (SPAC).

(1) SPEI

The SPEI was developed from the SPI, which describes the intensity and duration of droughts at different time scales. It considers not only the impact of precipitation but also the potential evapotranspiration factor influenced by temperature, and is widely used for the identification of monthly drought events [20]. The specific calculation process for the SPEI was as follows: (i) the Penman–Monteith method [41] was used to calculate the monthly cumulative potential evapotranspiration (PET); (ii) the difference between the monthly cumulative precipitation (Pc) and PET was used to calculate the water deficit (D); and (iii) the three-parameter log-logistic theory distribution function was selected to fit the D time series data and normalized. The SPEI calculation equation is as follows:

$$SPEI = W - \frac{C_0 + C_1 W + C_2 W^2}{1 + d_1 W + d_2 W^2 + d_3 W^3} \tag{1}$$

$$W = \sqrt{-2In(P)} \tag{2}$$

where P is the cumulative probability of exceeding the undetermined D value, when $P \leq 0.5$, $P = 1 - F(x)$; when $P > 0.5$, $P = 1 - P$. $C_0 = 2.515517$, $C_1 = 0.802853$, $C_2 = 0.010328$, $d_1 = 1.432788$, $d_2 = 0.189269$, $d_3 = 0.001308$. In general, SPEI values ranged from −2.5–2.5. A value of less than −0.5 is considered to be a drought event, and Table 2 illustrates the classification of drought levels based on SPEI [22,42].

Table 2. Classification of drought disaster levels.

Drought	Meteorological Index	Vegetation Index	Soil Index	Comprehensive Index
Disaster levels	SPEI	VHI	SMCI	CDI
None	(−0.5, +∞)	(0.4, 1]	(0.4, 1]	(−0.2, 1]
Light	(−1.0, −0.5]	(0.3, 0.4]	(0.3, 0.4]	(−0.2, −0.4]
Moderate	(−1.5, −1.0]	(0.2, 0.3]	(0.2, 0.3]	(−0.4, −0.6]
Severe	(−2.0, −1.5]	(0.1, 0.2]	(0.1, 0.2]	(−0.6, −0.8]
Extreme	(−∞, −2.0]	[0, 0.1]	[0, 0.1]	[−1, −0.8]

(2) VHI

VHI was developed to detect vegetation drought and consists of VCI and TCI, which are obtained from NDVI and BT, respectively; the lower the NDVI value and the higher the BT value, the poorer the vegetation health. The VHI considers the local biophysics (soil and slope) and climatic conditions. This method can be used for practical agro-drought monitoring in various agro-climatic zones. In particular, during crucial stages of crop growth, VHI and crop yield are strongly correlated [27].

$$VHI_i = \alpha \times VCI_i + (1 - \alpha) \times TCI_i \tag{3}$$

$$VCI_i = \frac{NDVI_i - NDVI_{min}}{NDVI_{max} - NDVI_{min}} \tag{4}$$

$$TCI_i = \frac{BT_{max} - BT_i}{BT_{max} - BT_{min}} \tag{5}$$

where $NDVI$, $NDVI_{max}$, and $NDVI_{min}$ (BT, BT_{max}, BT_{min}) are the smoothed $NDVI$ (BT) and the maximum and minimum values of $NDVI$ (BT) for each month in 1982–2020, respectively; and α represents the weighting coefficient of VCI. in this study, VHI correlates with SIF most closely when α = 0.7. The value of VHI ranges from 0 to 1, and the smaller the value, the more severe the vegetation drought. Kogan et al. [43,44] proposed that agricultural drought occurs when the VHI is less than 0.4, and the classification of drought levels based on the VHI [45] is shown in Table 2.

(3) SMCI

Agricultural drought is characterized primarily by insufficient soil moisture for plant root uptake and normal transpiration, which results in lower crop and pasture yields [30]. The SMCI, which describes drought in terms of soil moisture, is based on the standardization of the monthly mean values of root-zone soil moisture (SM) over a long time series. The calculation equation is as follows:

$$SMCI_i = \frac{SM_i - SM_{min}}{SM_{max} - SM_{min}} \tag{6}$$

where SM_i, SM_{max} and SM_{min} denote the root-zone soil moisture at time i and the maximum and minimum values of soil moisture during the same period from 1982 to 2020, respectively. The SMCI value is between 0 and 1. The calculation principle was the same as that of VCI, and the classification of the drought class based on SMCI [45] was identical to that of the VHI (Table 2).

(4) CDI

Based on the SPAC theory, the CDI developed from the response of meteorological drought, soil drought, and vegetation to drought was calculated using the following equations:

$$CDI = w_1 \times SPEI' + w_2 \times VHI' + w_3 \times SMCI' \tag{7}$$

$$SPEI' = SPEI/2.5 \tag{8}$$

$$SPEI = \begin{cases} 2.5 & SPEI \geq -2.5 \\ SPEI & 2.5 > SPEI > -2.5 \\ -2.5 & SPEI \leq -2.5 \end{cases} \tag{9}$$

$$VHI' = (VHI - 0.5) \times 2 \tag{10}$$

$$SMCI' = (SMCI - 0.5) \times 2 \tag{11}$$

where $SPEI'$, VHI', and $SMCI'$ represent the meteorological, vegetation and soil drought indicators after standardization of −1–1, respectively, and their drought classification criteria are the same as those of CDI (Table 1); the specific process of standardization is shown in Equation (8) to (11). The weights of each indicator, denoted by w_1, w_2, and w_3, are 0.12, 0.56, and 0.32, respectively.

2.3.2. Static and Dynamic Drought Hazard Models

Drought hazard is defined as the frequency and intensity of drought events [14]. Previous studies mostly weighted sums of drought frequencies with different severities to roughly represent drought hazards [15]. In this study, the CDI was used to identify droughts. The probability density curve of the CDI (Figure 3a) was used to construct a more accurate static hazard index, and the survival probability curve of CDI (Figure 3b) was used to construct a dynamic hazard index using the following equation:

$$Hazard = \int_{-1}^{-0.2} |PDF(CDI) \times CDI| \tag{12}$$

$$Hazard_i = \begin{cases} Hazard \times (1 - CDF(CDI_i)) & CDI_i \leq 0.2 \\ 0 & CDI_i > 0.2 \end{cases} \tag{13}$$

where *CDI* indicates the drought intensity, and *PDF(CDI)* is the probability density value, which denotes the probability of different *CDI* intensity. Because drought is considered to occur when *CDI* is less than −0.2, the accumulation of the absolute values of the products of *CDI* (from −1 to −0.2) and *PDF(CDI)* represents the multi-year (1982–2020) static hazard of a grid point; $Hazard_i$ denotes the drought hazard in year i; $CDF(CDI_i)$ denotes the cumulative probability of CDI_i, and $1 - CDF(CDI_i)$ is the survival probability. Based on the above method, we calculated the static and dynamic drought hazard for each grid point during the growing season (May to September) in NEC from 1982 to 2020 and standardized them so that the hazard values of all grid points fell between 0 and 1.

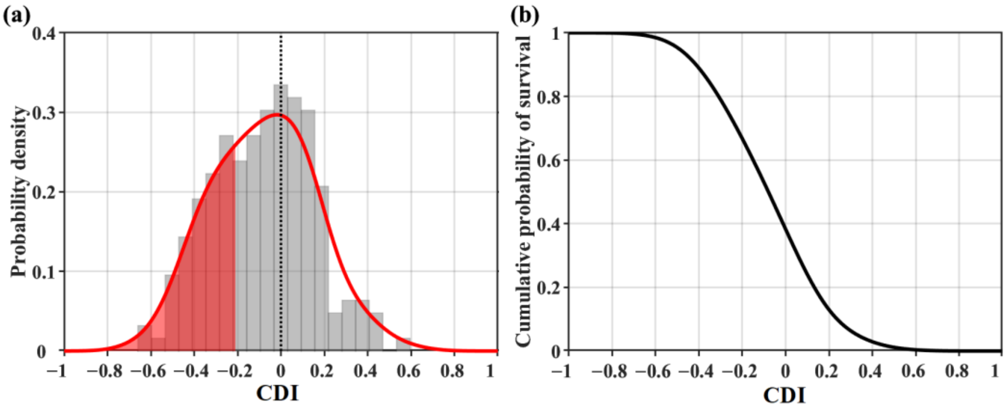

Figure 3. Probability density (**a**) and survival probability (**b**) distributions of the CDI.

2.3.3. Climatic Yield Anomalies

Crop yield may be influenced by the weather, pests, diseases, cultivation techniques, and management. To reflect the effect of climate change on crop yield, the Hodrick–Prescott (HP) filter method [46] was used to decompose crop yield (Y) into trend yield (Yt) and climatic yield (Yc). Yt reflects the long-period yield component of the agricultural production level, and Yc reflects the short-period yield component influenced by meteorological elements. (Yc/Yt) × 100% is the climatic yield anomalies, which is not affected by time, space and agricultural technology level, and is comparable among different regions.

2.3.4. Statistical Analysis

The correlation between SIF and various indices, such as scPDSI, SPEI, SMCI, VHI, and CDI under non-wet conditions (years with SPEI < 0.5), the correlation between drought-affected agricultural areas and various indices, and the correlation between climatic yield anomalies and drought hazard were examined using Pearson correlation analysis. The nonparametric Mann–Kendall (MK) test [47] was used to test the time-varying characteristics of various indices, where UF (UB) is the sequence (inverse) statistic of the time series data. Sen's slope estimation and the MK trend significance test [48,49] were used for the trend variation and significance analysis of each index in space. The direction of the trend is indicated by the sign of the Z value in the MK trend significance test results; a positive Z value indicates an upward trend and vice versa. When $|Z| > 1.96$, a significant trend was observed at the 5% significance level.

3. Results and Discussion

3.1. Construction of the CDI

3.1.1. Response of SIF to Different Drought Indices

The results of the correlation analysis between various drought indices and SIF during the growing season in NEC from 2000 to 2020 (Figure 4a–g) showed that each drought index in the study area was mainly positively correlated with SIF (more than 80.9% of grids), especially in farmland and grassland, and the significant ($p < 0.05$) positively correlated regions were mainly distributed in the central and western part of the study area, indicating that drought would suppress photosynthesis in crops. The proportion of grids with a positive correlation of VCI, VHI and CDI with SIF in the NEC exceeded 98.6%, probably because VCI and SFI are both vegetation indices of remote sensing inversion, and the contribution of VCI to VHI and CDI is larger, with the weight of VCI constituting VHI being 0.7, and the weight of VHI constituting CDI being 0.56. In some woodland areas, there was a negative correlation between SIF and TCI, SPEI, SMCI, and scPDSI. This is likely because forests are more resilient to short-term droughts than are crops and grass. When the main factor limiting photosynthesis in plants is not water, temperature and rainy weather with precipitation will lead to lower temperatures and reduced radiation, thus limiting photosynthesis in forests, which also indicates that these drought indices are more applicable in farmland and grassland than in woodland. In contrast, CDI and SIF were predominantly significantly and positively correlated in the forest region, suggesting that the comprehensive index extends the applicability of drought monitoring to some extent. The statistical results of the correlation analysis between each index and SIF in the farmland and grassland areas (Figure 4h) showed that the correlation between SIF and VHI (r = 0.58) increased compared to VCI (r = 0.56) after considering TCI. The correlation between SIF and SPEI (r = 0.12) was the weakest, followed by SMCI (r = 0.49). The correlation between SIF and CDI (r = 0.65) was the strongest correlation and was significantly higher than that of the commonly used drought index scPDSI (r = 0.24), indicating that CDI combines the advantages of soil, vegetation, and meteorological drought indices; considers the effect of temperature on drought; and can be used for agricultural drought identification in NEC.

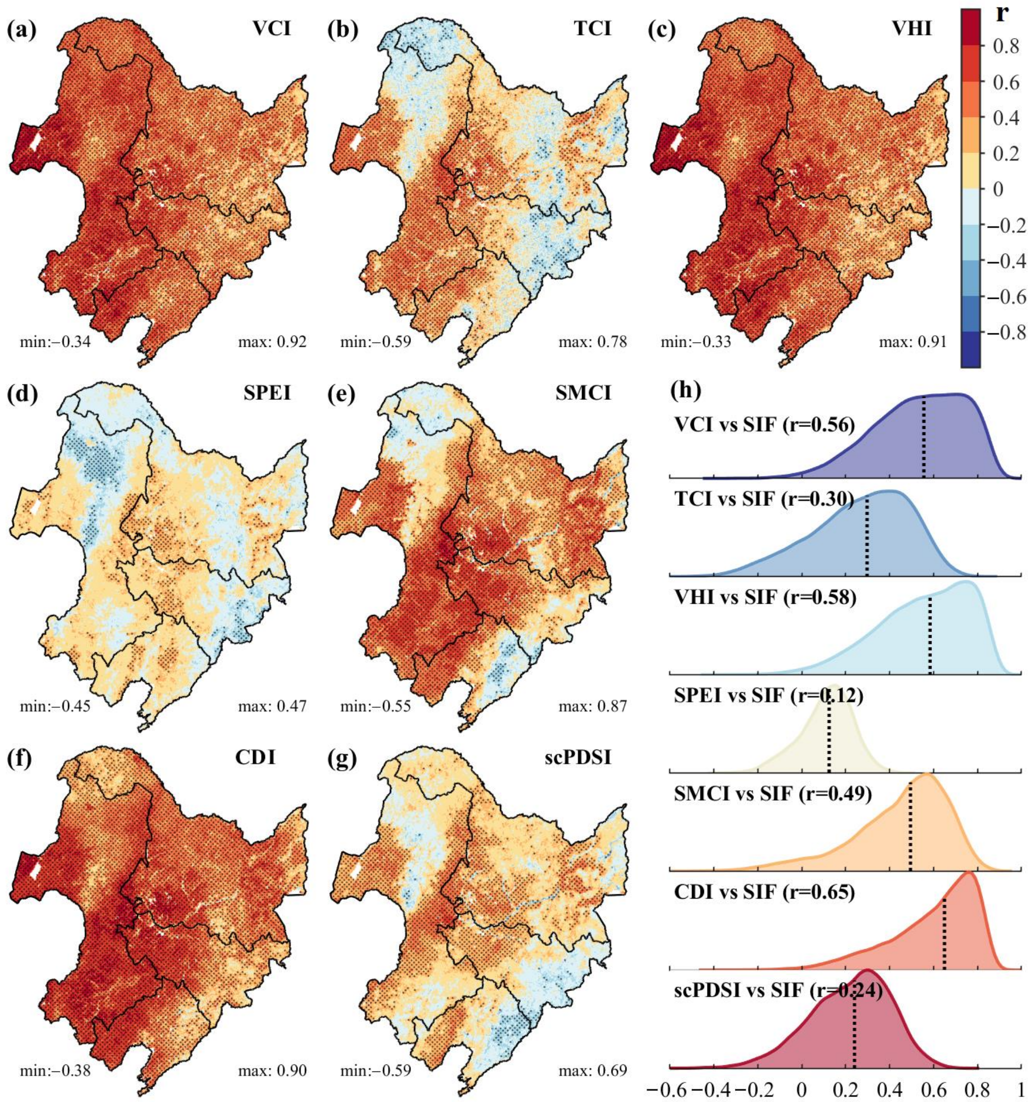

Figure 4. Correlations (**a**–**g**) and statistics (**h**) of different drought indices with SIF in NEC, 2000–2020. (Dotted areas indicate $p < 0.05$ significant correlations, dashed lines indicate median correlation coefficients of all grid points in farmland and grassland areas.)

3.1.2. Comparison of Temporal Variation of Different Drought Indices

The characteristics of the temporal variation in the different drought indices from 1982 to 2020 (Figure 5) were highly similar, showing a decreasing trend followed by an increasing trend. The UB curve of the MK test shows that the trend of each index turned around 2000. All indices showed a decreasing trend, except for VHI, which showed a non-significant ($p < 0.05$) increasing trend. This is probably because NEC is located in the middle and high latitudes, where the lack of heat resources is one of the factors limiting the growth and development of crops, and warming, combined with relatively sufficient moisture, instead promoted crop production. The scPDSI had the best correlation with SMCI (r = 0.81), followed by SPEI (r = 0.75) and the weakest correlation with VHI (r = 0.44). The scPDSI was less similar to the temporal variation characteristics of the CDI by VHI than SMCI, but still significantly correlated (r = 0.76, $p < 0.01$). The SPEI, VHI, SMCI, and scPDSI have been used to reflect the spatial and temporal variation of agricultural drought characteristics in NEC, and several studies are consistent with our findings [1,50–55]. Xue et al. [51] found that the moment of trend shift of SPEI12 in NEC was around 2000, after which the drought trend eased, and the drought area showed a decreasing trend. After 2000, the annual precipitation in NEC increased, and the average annual temperature decreased, while it also showed a trend of greening and productivity growth [52,56]. Because of the significant decrease in ET0, NEC has experienced significant climatic wetting, which could alleviate the agricultural drought crisis [55]. Ecological improvements from forest and cropland protection policies [56] and the seasonal dependence of the Atlantic sea surface temperature (SST) and atmospheric circulation [57] have improved climatic conditions in NEC, resulting in a decreasing trend of agricultural drought hazard in the last 20 years.

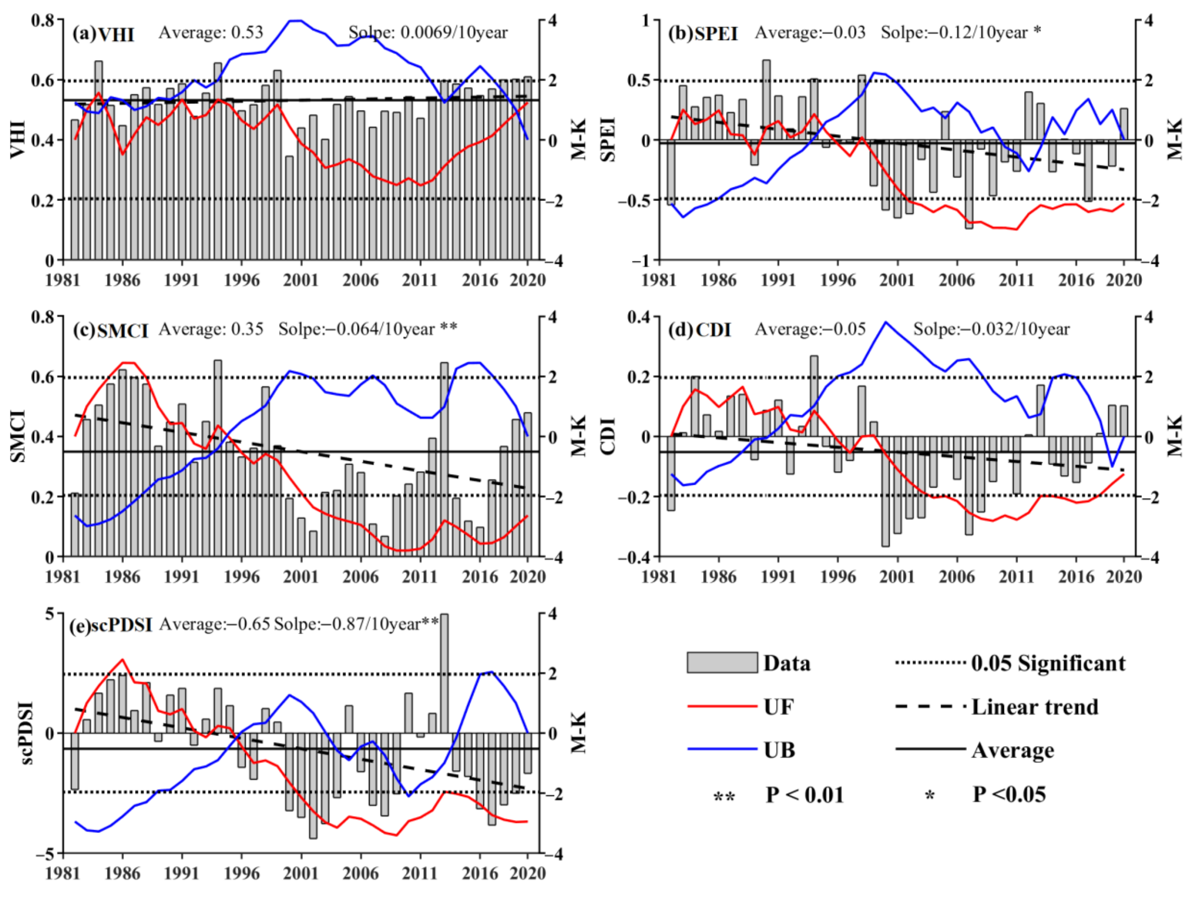

Figure 5. Temporal variation of different drought indices in the growing season of crops in NEC from 1982 to 2020 (**a**–**e**).

3.1.3. Response of Agricultural Drought-Affected Area to Different Drought Indices

We examined the temporal variation in the drought-affected area of agriculture and various drought indices of farmland areas in the study area from 1986 to 2015 to compare their applicability to agricultural drought in NEC (Figure 6). The results revealed that the drought-affected area was highly significantly ($p < 0.001$) and correlated with each drought index, with the CDI (r = −0.732) best reflecting the impact of drought on agriculture and much better than the scPDSI (r = −0.639). Among the soil, atmospheric, and vegetation drought indices, SMCI (r = −0.712) had the highest correlation, indicating that a soil moisture deficit is most critical in agricultural drought. The VHI (r = −0.584) has the worst correlation with the drought-affected area of agriculture, and this may be because the reduction in VHI is not only due to drought, but also other meteorological disasters or pests. In addition, factors such as coarse resolution (crops mixed with forests in one pixel) and cloud pollution can also affect the accuracy of the VHI in monitoring agricultural drought. Considering the response relationship of each drought index with SIF and the agricultural drought area, we discovered that the CDI has the advantages of wide spatial range, long time range, and high accuracy in drought identification, which can be used for further study of agricultural drought hazards in NEC.

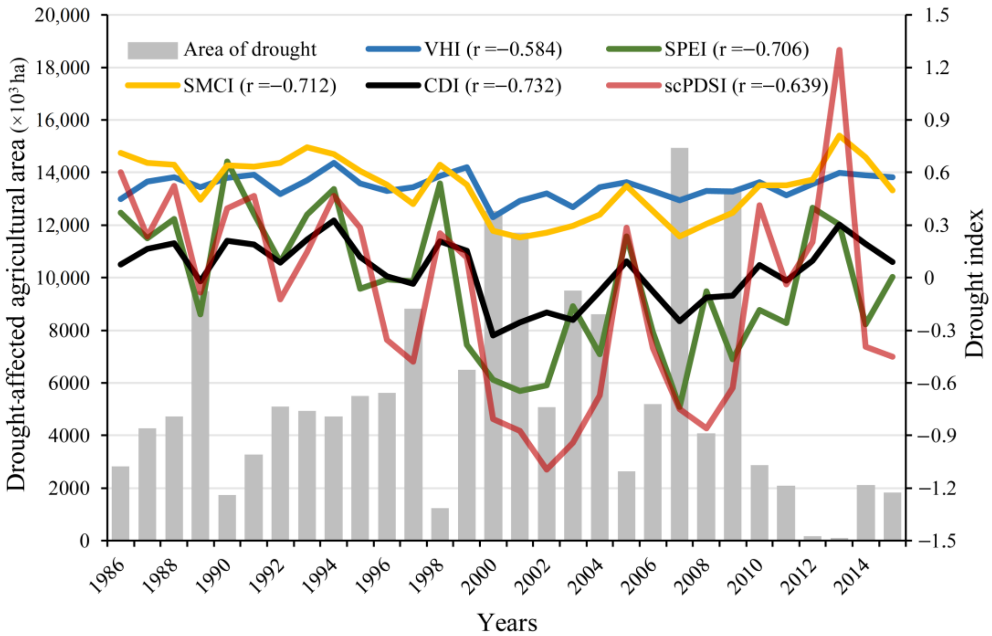

Figure 6. Temporal variation of drought-affected area of agriculture and different drought indices for farmland in NEC, 1986–2015. (The scPDSI value typically ranges from −4 to 4, and here it is divided by 4.)

3.2. Spatial and Temporal Variation of Drought in NEC Based on CDI

The spatial pattern of the CDI trends in the NEC growing season was obtained by using Sen's slope and the MK significance test in three time periods: 1982–2020, 1982–1999, and 2000–2020, and the statistics were conducted by vegetation type (Figure 7). This analysis revealed that while there was clear spatial heterogeneity in CDI trends across time periods, there was some similarity between the different months of the growing season. During 1982–2020 (Figure 7a), the CDI primarily decreased in the western part of the study area, while it increased in the central and eastern parts. There, CDI significantly decreased in the western part of the study area in July, August, and September, with the largest number of significantly decreasing grid points in August. CDI trends were mostly downward throughout the study area, but in farmland (Figure 7d), the proportion of grids with decreasing trends decreased with each passing month, from 64.6% in May to 30.0% in September, with mainly downward trends (becoming dry) in May and June, and mainly upward trends (becoming wet) from July to September. The trend of CDI in the study area shifted significantly around 2000 (Figure 7b–d), with farmland, woodland, and grassland cover areas dominated by a non-significant decrease from 1982 to 1999 and a significant increase from 2000 to 2020. However, some of the regional CDI trends remained consistent in both time periods, while the southwestern region of the study area experienced an upward trend in CDI during various months of the growing season during both periods, whereas the northwestern and southeastern regions experienced an opposite trend. The range of CDI trends for both periods before and after 2000 was higher than that of 1982–2020 (Figure 7a–c), indicating that later wetting suppressed the trend of drying throughout the period. Areas of significant changes in CDI trends over the three time periods were mostly found in farmland and grassland areas, indicating that dry/wet conditions and vegetation growth in these areas are more susceptible to climate change.

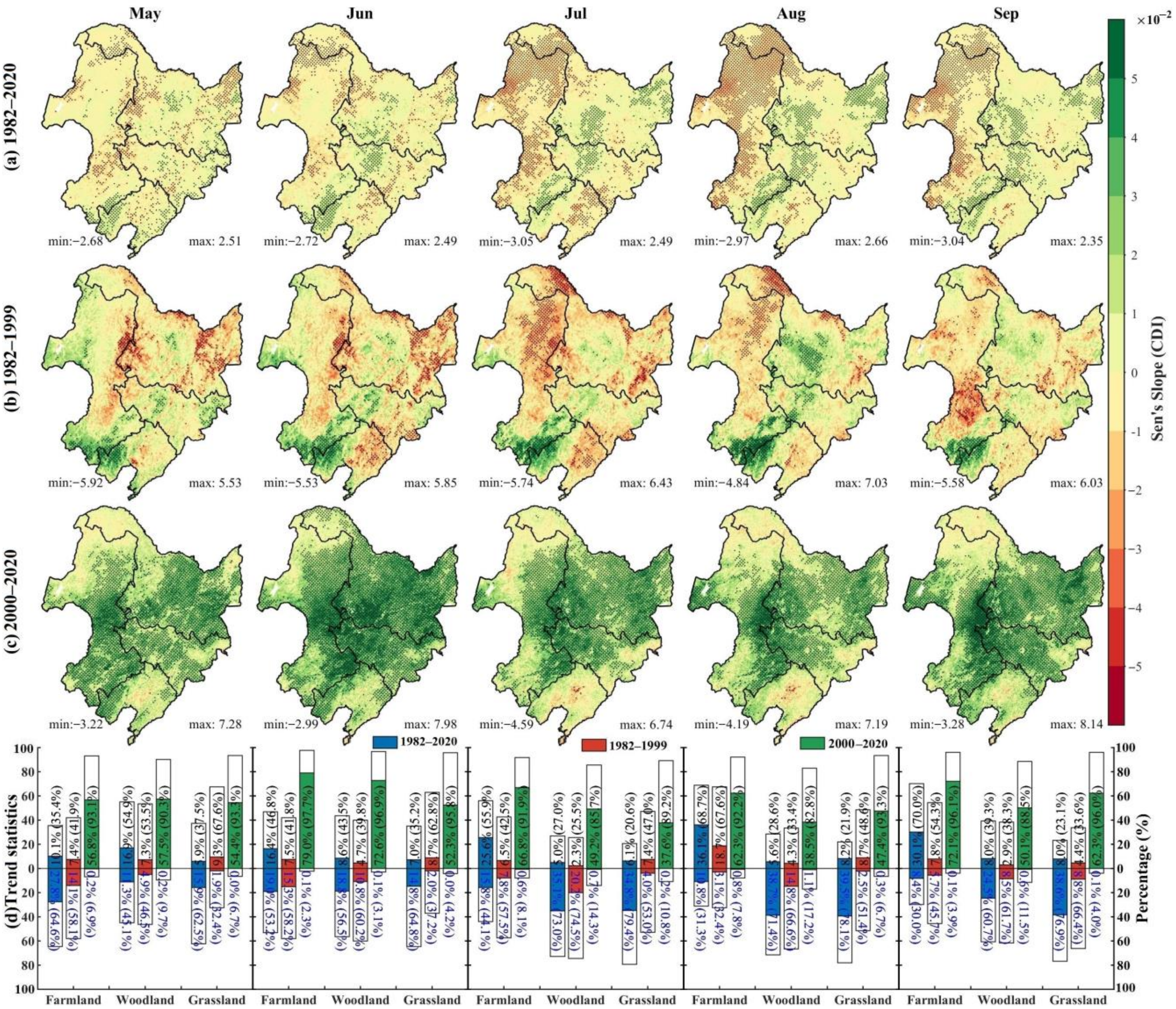

Figure 7. Spatial pattern (**a**–**c**) and statistics (**d**) of CDI trends during the growing season in NEC at different periods. (Dotted area indicates an MK significance test of |Z| > 1.96; the upper part of the bar graph indicates the proportion of the grid with an increasing trend, and the colored part indicates the proportion of the grid with significant change.)

According to the drought levels classified by the CDI, the spatial distribution of drought frequencies of varying severity during the growing season in NEC from 1982 to 2020 is presented (Figure 8). The results showed that the frequency decreased with increasing drought intensity. May and June had more drought occurrences than July through September. The western and eastern regions of the study area have a high frequency of light drought, while the central farmland and southern grassland regions have a high frequency of moderate, severe and extreme drought. Severe and extreme drought disasters rarely occur in woodlands. On the one hand, forest ecosystems are complex and have a high stability of resistance [48], and on the other hand, the CDI is a short-term drought monitoring indicator, which is more suitable to reflect agricultural drought.

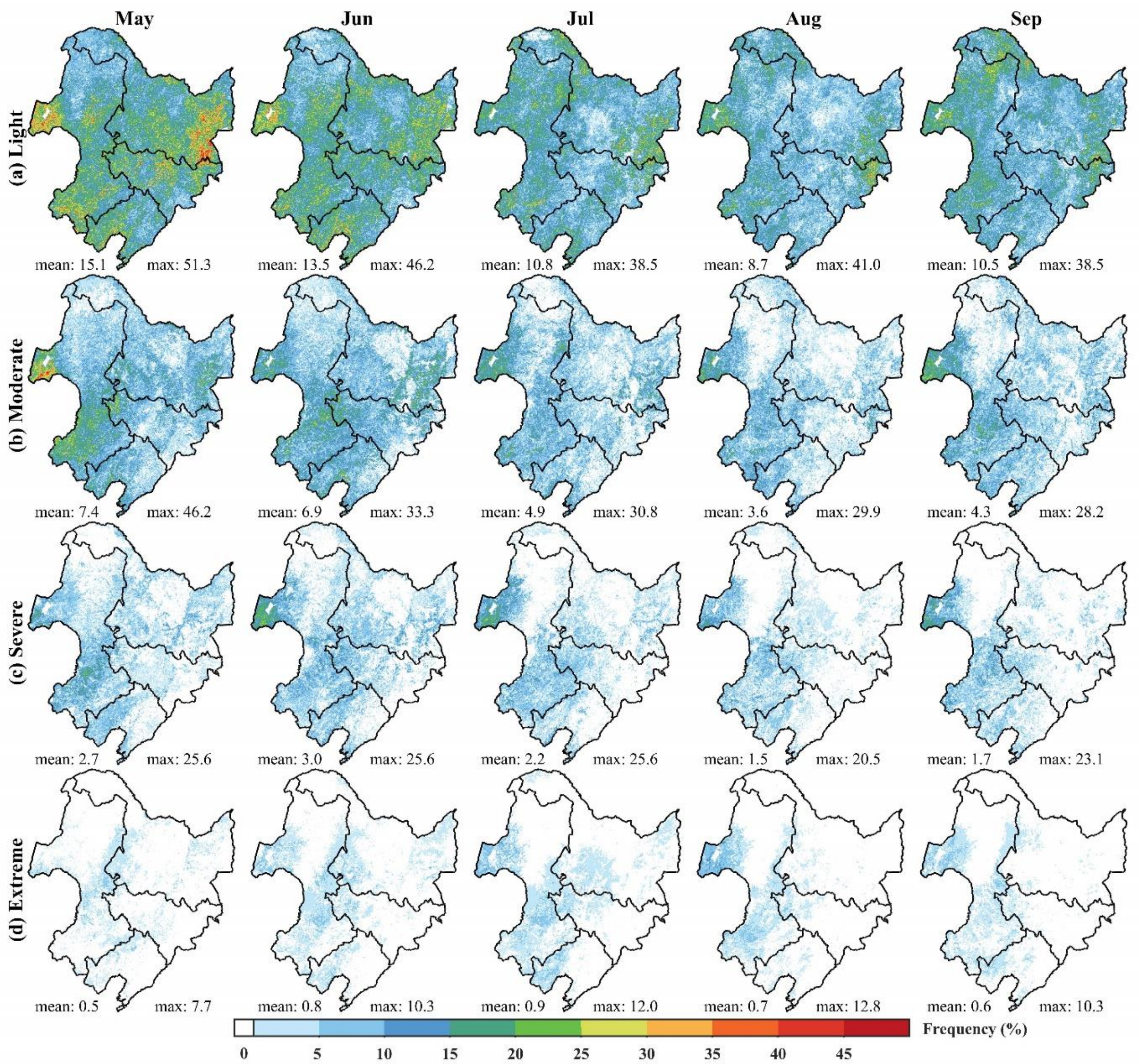

Figure 8. Spatial pattern of different drought level frequencies based on the CDI in the growing season of NEC from 1982 to 2020.

The impact of different levels of drought during the growing season of farmland and grassland in NEC from 1982 to 2020 (Figure 9) showed that agricultural drought events in different months of the growing season were mainly concentrated in 2000–2009, with light and moderate drought dominating before 2000 and after 2009, and the impact scope of severe and extreme drought increasing greatly from 2000 to 2009. The average drought impact scopes were 30.5%, 29.3%, 21.4%, 16.8% and 19.5% from May to September, respectively, which indicated that the farmland and grassland in NEC was most severely affected by spring drought, and it was the main factor limiting crop sowing and the cultivation of strong seedlings. The year 2000 had the highest average drought impact scope (67.4%) during the growing season, which had abnormally high temperatures and little rain around June and July. The drought lasted for a long time with high intensity, which exacerbated the adverse effects of drought on crops in the absence of sufficient water [6]. This caused serious consequences, and the grain yield was reduced by more than 30% in the majority of areas. Therefore, based on the CDI, drought hazard evaluation is important for the government and farmers to formulate relevant disaster prevention and mitigation strategies and reduce drought losses.

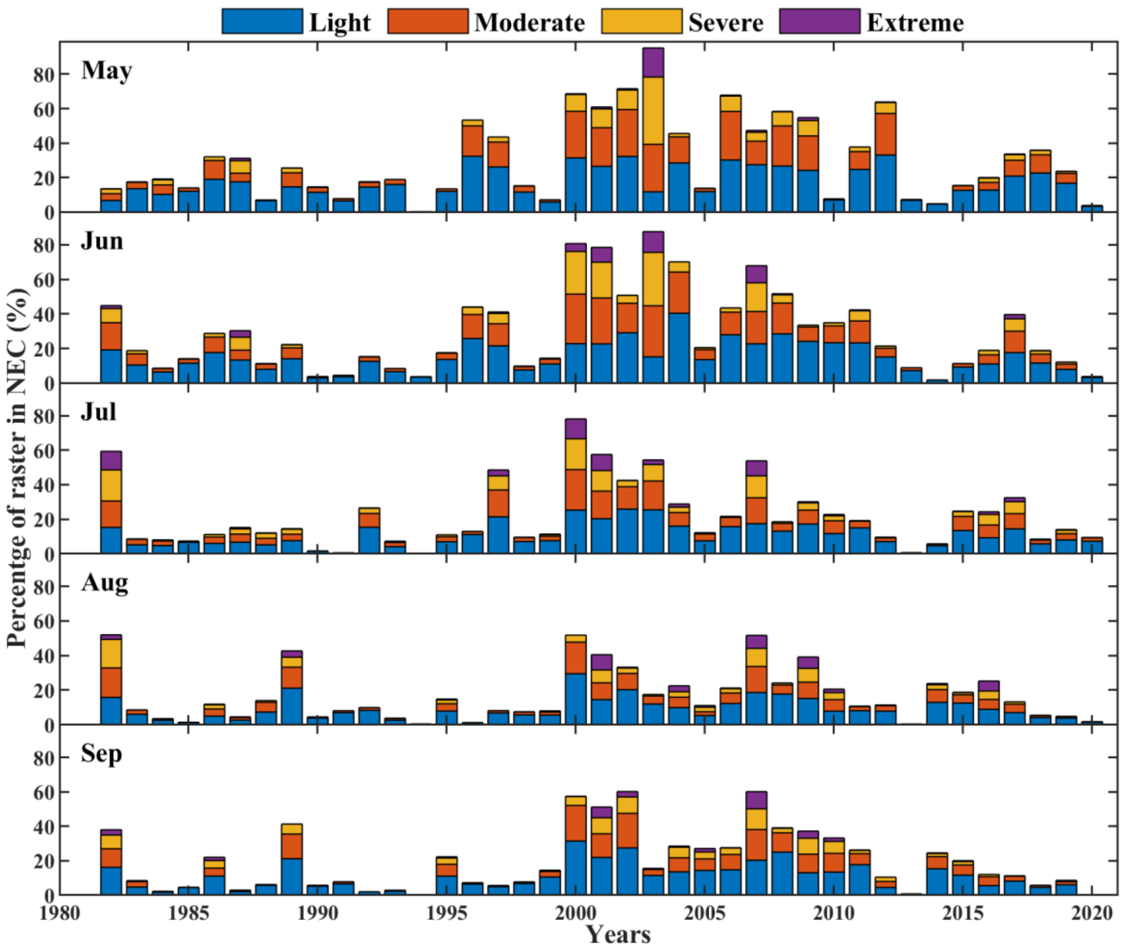

Figure 9. Temporal changes in drought impact scope based on the CDI during the growing season in NEC from 1982 to 2020.

3.3. Quantitative Evaluation of Agricultural Drought Hazard in NEC Based on CDI

The static drought hazard for NEC was determined grid by grid for the years 1982 to 2020 using CDI and the static hazard evaluation model. To determine the agricultural drought hazard class thresholds (Table 3) in the growing season of NEC, the dynamic hazard of CDI at −0.2, −0.4, −0.6, and −0.8 was calculated for each grid point based on the CDI thresholds for drought levels (Table 2), and the 20%, 40%, 60%, and 80% quartiles of these hazards for all grid points in farmland and grassland areas were also counted. Figure 10 shows the spatial pattern of various agricultural drought hazard levels during the growing season in NEC and the statistical results. The high and above hazard areas were mainly concentrated in the grassland and farmland areas in the west-central and northeastern parts of the study area, whereas the extra-low hazard areas were primarily distributed in the wet zone and woodland areas in the eastern part of the study area. The woodland area was dominated by very low and low hazards, the grassland area was dominated by moderate and above hazards, and the farmland area was in between. For crop layout adjustments, irrigation project building, and the design of policies for disaster prevention and mitigation in NEC, the outcomes of the static drought hazard evaluation serve as significant reference values.

Table 3. Agricultural drought hazard level thresholds for the growing season of crops in NEC.

Hazard Levels	May	Jun	Jul	Aug	Sep
Extra-low	[0, 0.206)	[0, 0.192)	[0, 0.151)	[0, 0.104)	[0, 0.136)
Low	[0.206, 0.335)	[0.192, 0.335)	[0.151, 0.247)	[0.104, 0.173)	[0.136, 0.218)
Moderate	[0.335, 0.475)	[0.335, 0.465)	[0.247, 0.348)	[0.173, 0.260)	[0.218, 0.301)
High	[0.475, 0.651)	[0.465, 0.629)	[0.348, 0.494)	[0.260, 0.397)	[0.301, 0.429)
Extra-high	[0.651, 1]	[0.629, 1]	[0.494, 1]	[0.397, 1]	[0.429, 1]

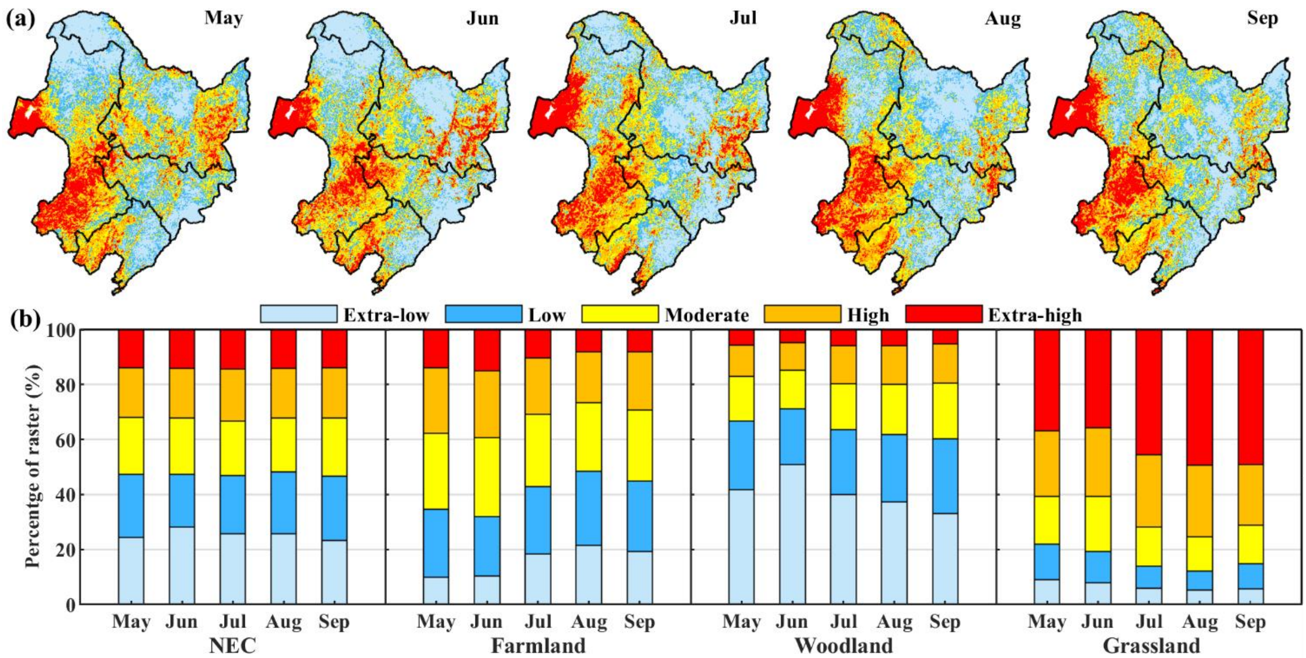

Figure 10. Spatial pattern of various levels of static agricultural drought hazard (**a**) and statistics (**b**) during the growing season in NEC.

The dynamics of agricultural drought hazard in farmland and grassland areas (Figure 11) revealed that the drought hazard increased non-significantly ($p < 0.05$) over the course of different months from 1982 to 2020, with the largest increasing trend in May at 0.021/10 years. According to the results of the MK test, the drought hazard trend changed significantly around 2000; the hazard trend from 1982 to 1999 did not reach a significant ($p < 0.05$) level, and all months from 2000 to 2020 showed a significant ($p < 0.01$) decreasing trend, with the largest trend of $-0.153/10$ years in June. With a warming climate and frequent drought events, the hazard of drought increased significantly after 2000. During the growing season, the hazard generally decreased as the months increased but was noticeably higher in May and June than in other months. The years of high drought hazard were concentrated in 2000–2009, when there was also a period of high incidence of drought events in NEC (Figure 9). During the crop-growing season (May–September) in NEC, precipitation is lowest in May, and droughts induced by a combination of low precipitation and high temperatures frequently occur in spring and autumn [9,51]. May is the sowing and seedling stage of crops in NEC. During this period, drought delays sowing, inhibiting the growth rate of crop seedlings and reducing biomass, leaf area index (LAI), and chlorophyll content; prolonged drought can even lead to seedling death, forcing farmers to replant [58]. Therefore, the drought hazard index was highest in May.

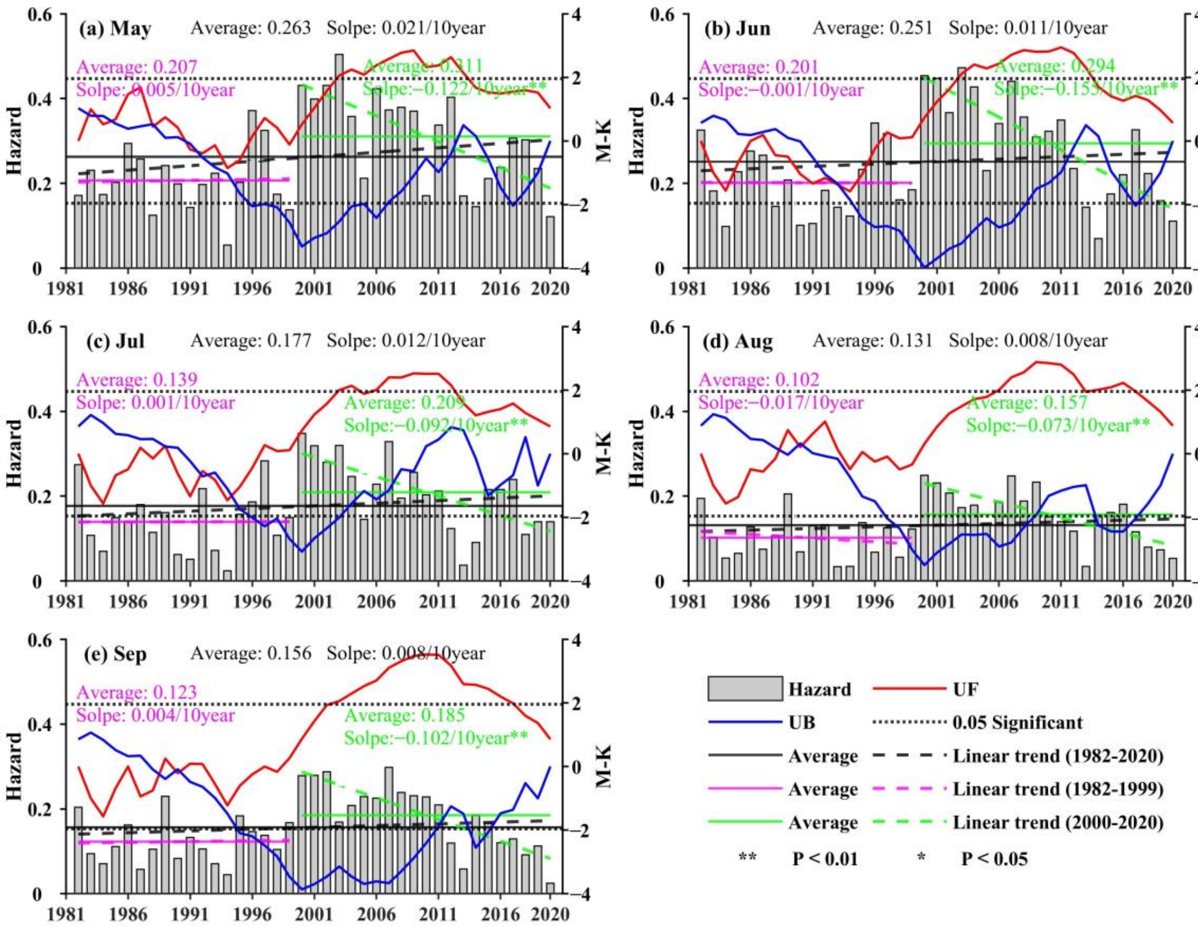

Figure 11. Temporal variation of drought hazard during the growing season in NEC, 1982–2020 (**a**–**e**).

3.4. Validation of Hazard Assessment Models

The largest rain-fed maize-producing region in China is NEC [59], with maize production accounting for 38.9% of the total national grain production. The study area has the largest area under maize cultivation, accounting for 49.2% of the total area under all crops (National Bureau of Statistics of China, 2020). Therefore, we selected maize as a representative crop in the study area to analyze the linear relationship between climatic yield anomalies and drought hazards during the growing season (Figure 12). The results showed that increasing drought risk reduced climatic yield anomalies. The drought hazard index was highly significantly ($p < 0.001$) negatively correlated with climatic yield anomalies in all months, except May. The seedling emergence of maize occurred in May, when the occurrence of drought had a weaker effect on the final maize yield. The effect of drought hazard on climatic yield anomalies was much higher in July and August than in the other months when maize was in the flowering and filling stage, a critical period for grain and yield formation [12]. The drought hazard in August explained 28% ($R^2 = 0.28$) of the variation in maize yield. NEC is also the main soybean-producing area in China, and soybean cultivation is mainly concentrated in Heilongjiang Province. Soybeans (Figure S1) in Heilongjiang Province showed the same results as maize (Figure 12) in NEC. Wang et al. [31] showed that moisture anomalies (drought and flooding) explain 34% of the variation in maize yield, which is similar to the results of this study. The first step in risk analysis is hazard assessment, and the hazard findings in this study reflect the actual situation of drought impact on crop yield. One of the primary barriers to high and stable maize yield in NEC is drought risk [60]. Studies have shown that combined heat and drought stress is a major factor limiting maize yield [34], which means that drought risk may further increase as the climate warms and extreme weather events increase. Dynamic drought risk assessments are necessary for emergency drought mitigation, in addition to static drought risk assessments that serve as a roadmap for planning drought prevention and response strategies [61]. The knowledge gained from this study can serve as a technical support and foundation for dynamic risk assessment and management.

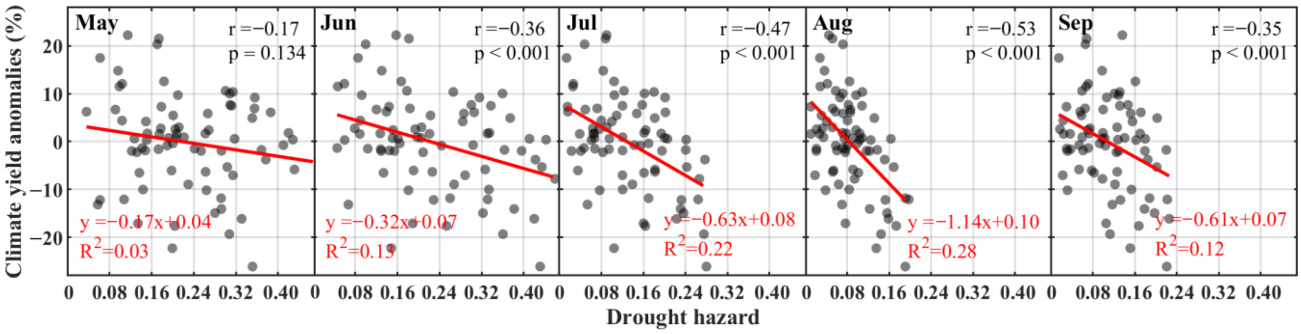

Figure 12. Linear relationship between climatic yield anomalies and drought hazard during the growing season for maize in NEC.

3.5. Limitations

Several studies have demonstrated that a comprehensive index that incorporates multi-source information and multi-sensor data can effectively monitor agricultural drought and assess its impacts [1,26,30,31,45]. SIF data, which are more sensitive to changes in water and heat, were used in this study as the basis to build the CDI, which increased the sensitivity of drought monitoring but also restricted the use of the CDI. In comparison to grassland and farmland, the CDI was less reliable for drought monitoring in woodlands and better suited for short-term drought monitoring. The accuracy of the CDI for monitoring agricultural drought is also weakened by the presence of mixed pixels in remote sensing data, which can be strengthened by higher-resolution remote sensing data in the following step. The growing season used in this study was from May to September; however, since drought is a continuous occurrence and the actual sowing and harvesting dates for each grid in the study area vary by region, year, and crop type, more research is needed to determine the relationship between drought hazard and yield loss for specific crops by improving the temporal resolution of the data.

4. Conclusions

Based on SPAC theory, this study integrated multi-source information data such as meteorology, remote sensing, and reanalysis, to construct a comprehensive drought index. Through static and dynamic hazard assessment models, we analyzed the spatial and temporal distribution characteristics of drought disaster and hazard during the growing season (May to September) in NEC and also verified the validity of the CDI and hazard index. The following conclusions were obtained:

(1) Compared with a single drought index, the CDI index for drought monitoring has the advantages of a broad spatial range, long time range, and high accuracy and can reflect agricultural drought well.

(2) The growing season in NEC showed a trend of becoming drier from 1982 to 2020, and the hazard of agricultural drought also showed a non-significant ($p < 0.05$) increasing trend. However, the trends of the drought index, the impact scope of drought events, and the hazard of agricultural drought all turned around 2000, and the drought hazard was highly significant ($p < 0.001$) and decreased from 2000 to 2020.

(3) The frequency of drought disasters was the highest and the hazard was the highest in May. The best level of climatic yield anomalies in maize was explained by the drought hazard in August ($R^2 = 0.28$). High hazard levels were mostly distributed in the farmland and grassland areas located in the central and western parts of the study area.

Supplementary Materials: The following supporting information can be downloaded at: https://www.mdpi.com/article/10.3390/rs15010057/s1, Figure S1. Linear relationship between climatic yield anomalies and drought hazard during the growing season (May to September) for soybean in Heilongjiang Province.

Author Contributions: Conceptualization, K.L. and J.Z.; methodology, K.L. and G.R.; data, B.S. and Q.S.; validation, S.W., C.L., Y.Y. and Y.G.; writing—original draft preparation, K.L.; writing—review and editing, J.Z.; project administration, J.Z.; funding acquisition, J.Z. and C.W. All authors have read and agreed to the published version of the manuscript.

Funding: This study was supported by the National K&D Program of China (2019YFD1002201), the National Natural Science Foundation of China (U21A2040), the National Natural Science Foundation of China (41877520), the National Natural Science Foundation of China (42077443). Industrial technology research and development Project of Development and Reform Commission of Jilin Province (2021C044-5), the Key Scientific and Technology Research and Development Program of Jilin Province (20200403065SF), and the Construction Project of the Science and Technology Innovation Center (20210502008ZP).

Conflicts of Interest: The authors declare no conflict of interest.

References

1. Zhang, Y.; Liu, X.; Jiao, W.; Zeng, X.; Xing, X.; Zhang, L.; Yan, J.; Hong, Y. Drought monitoring based on a new combined remote sensing index across the transitional area between humid and arid regions in China. *Atmos. Res.* **2021**, *264*, 105850. [CrossRef]
2. IPCC. *Climate Change 2021: The Physical Science Basis. Contribution of Working Group I to the Sixth Assessment Report of the Intergovernmental Panel on Climate Change*; Masson-Delmotte, V., Zhai, P., Pirani, A., Connors, S.L., Péan, C., Berger, S., Caud, N., Chen, Y., Goldfarb, L., Gomis, I., et al., Eds.; Cambridge University Press: Cambridge, UK; New York, NY, USA, 2021.
3. WMO. *WMO Provisional Report on the State of the Global Climate 2020*; World Meteorological Organization: Geneva, Switzerland, 2020.
4. Li, E.; Zhao, J.; Pullens, J.W.; Yang, X. The compound effects of drought and high temperature stresses will be the main constraints on maize yield in Northeast China. *Sci. Total. Environ.* **2022**, *812*, 152461. [CrossRef] [PubMed]
5. Li, H.; He, S.; Gao, Y.; Chen, H.; Wang, H. North Atlantic Modulation of Interdecadal Variations in Hot Drought Events Over Northeastern China. *J. Clim.* **2020**, *33*, 4315–4332. [CrossRef]
6. Li, H.; Chen, H.; Sun, B.; Wang, H.; Sun, J. A Detectable Anthropogenic Shift Toward Intensified Summer Hot Drought Events Over Northeastern China. *Earth Space Sci.* **2020**, *7*, e2019EA000836. [CrossRef]
7. Chen, D.; Gao, Y.; Sun, J.; Wang, H.; Ma, J. Interdecadal Variation and Causes of Drought in Northeast China in Recent Decades. *J. Geophys. Res. Atmos.* **2020**, *125*, e2019JD032069. [CrossRef]
8. Zhao, Z.; Wang, H.; Yu, C.; Deng, C.; Liu, C.; Wu, Y.; Yan, J.; Wang, C. Changes in spatiotemporal drought characteristics over northeast China from 1960 to 2018 based on the modified nested Copula model. *Sci. Total Environ.* **2020**, *739*, 140328. [CrossRef]
9. Wang, C.; Linderholm, H.W.; Song, Y.; Wang, F.; Liu, Y.; Tian, J.; Xu, J.; Song, Y.; Ren, G. Impacts of Drought on Maize and Soybean Production in Northeast China during the Past Five Decades. *Int. J. Environ. Res. Public Health* **2020**, *17*, 2459. [CrossRef]
10. Xie, W.; Xiong, W.; Pan, J.; Ali, T.; Cui, Q.; Guan, D.; Meng, J.; Mueller, N.D.; Lin, E.; Davis, S. Decreases in global beer supply due to extreme drought and heat. *Nat. Plants* **2018**, *4*, 964–973. [CrossRef]
11. Yin, X.G.; Olesen, J.E.; Wang, M.; Öztürk, I.; Chen, F. Climate effects on crop yields in the Northeast Farming Region of China during 1961–2010. *J. Agric. Sci.* **2016**, *154*, 1190–1208. [CrossRef]
12. Yu, X.; He, X.; Zheng, H.; Guo, R.; Ren, Z.; Zhang, D.; Lin, J. Spatial and temporal analysis of drought risk during the crop-growing season over northeast China. *Nat. Hazards* **2014**, *71*, 275–289. [CrossRef]
13. Yang, Y.; Wei, S.; Li, K.; Zhang, J.; Wang, C. Drought risk assessment of millet and its dynamic evolution characteristics: A case study of Liaoning Province, China. *Ecol. Indic.* **2022**, *143*, 109407. [CrossRef]
14. Zhang, Q.; Zhang, J.; Wang, C. Risk assessment of drought disaster in typical area of corn cultivation in China. *Theor. Appl. Climatol.* **2017**, *128*, 533–540. [CrossRef]
15. Geng, G.; Wu, J.; Wang, Q.; Lei, T.; He, B.; Li, X.; Mo, X.; Luo, H.; Zhou, H.; Liu, D. Agricultural drought hazard analysis during 1980-2008: A global perspective. *Int. J. Climatol.* **2016**, *36*, 389–399. [CrossRef]
16. McCarthy, J.J.; Canziani, O.F.; Leary, N.A.; Dokken, D.J.; White, K.S. *Climate Change 2001: Impacts, Adaptation, And Vulnerability: Contribution of Working Group II to the Third Assessment Report of the Intergovernmental Panel on Climate Change*; Cambridge University Press: Cambridge, UK, 2001.
17. Kim, H.; Park, J.; Yoo, J.; Kim, T.-W. Assessment of drought hazard, vulnerability, and risk: A case study for administrative districts in South Korea. *J. Hydro-Environ. Res.* **2015**, *9*, 28–35. [CrossRef]
18. Cheval, S.; Dumitrescu, A.; Birsan, M.-V. Variability of the aridity in the South-Eastern Europe over 1961–2050. *Catena* **2017**, *151*, 74–86. [CrossRef]

19. van der Schrier, G.; Barichivich, J.; Briffa, K.R.; Jones, P.D. A scPDSI-based global data set of dry and wet spells for 1901–2009. *J. Geophys. Res. Atmos.* **2013**, *118*, 4025–4048. [CrossRef]
20. Vicente-Serrano, S.M.; Beguería, S.; López-Moreno, J.I. A Multiscalar Drought Index Sensitive to Global Warming: The Standardized Precipitation Evapotranspiration Index. *J. Clim.* **2010**, *23*, 1696–1718. [CrossRef]
21. Wells, N.; Goddard, S.; Hayes, M.J. A self-calibrating Palmer drought severity index. *J. Clim.* **2004**, *17*, 2335–2351. [CrossRef]
22. McKee, T.B.; Doesken, N.J.; Kleist, J. The relationship of drought frequency and duration to time scales. In Proceedings of the Eighth Conference on Applied Climatology, Anaheim, CA, USA, 17–22 January 1993; Volume 17, pp. 179–183.
23. Carlson, T.N.; Ripley, D.A. On the relation between NDVI, fractional vegetation cover, and leaf area index. *Remote Sens. Environ.* **1997**, *62*, 241–252. [CrossRef]
24. Zambrano, F.; Lillo-Saavedra, M.; Verbist, K.; Lagos, O. Sixteen Years of Agricultural Drought Assessment of the BioBío Region in Chile Using a 250 m Resolution Vegetation Condition Index (VCI). *Remote Sens.* **2016**, *8*, 530. [CrossRef]
25. Bhuiyan, C.; Singh, R.; Kogan, F. Monitoring drought dynamics in the Aravalli region (India) using different indices based on ground and remote sensing data. *Int. J. Appl. Earth Obs. Geoinf.* **2006**, *8*, 289–302. [CrossRef]
26. Zhang, A.; Jia, G. Monitoring meteorological drought in semiarid regions using multi-sensor microwave remote sensing data. *Remote Sens. Environ.* **2013**, *134*, 12–23. [CrossRef]
27. Bento, V.A.; Gouveia, C.M.; DaCamara, C.C.; Trigo, I.F. A climatological assessment of drought impact on vegetation health index. *Agric. For. Meteorol.* **2018**, *259*, 286–295. [CrossRef]
28. Jiao, W.; Wang, L.; Smith, W.K.; Chang, Q.; Wang, H.; D'Odorico, P. Observed increasing water constraint on vegetation growth over the last three decades. *Nat. Commun.* **2021**, *12*, 3777. [CrossRef] [PubMed]
29. Williamson, S.N.; Hik, D.; Gamon, J.; Kavanaugh, J.L.; Koh, S. Evaluating Cloud Contamination in Clear-Sky MODIS Terra Daytime Land Surface Temperatures Using Ground-Based Meteorology Station Observations. *J. Clim.* **2013**, *26*, 1551–1560. [CrossRef]
30. Xu, L.; Abbaszadeh, P.; Moradkhani, H.; Chen, N.; Zhang, X. Continental drought monitoring using satellite soil moisture, data assimilation and an integrated drought index. *Remote Sens. Environ.* **2020**, *250*, 112028. [CrossRef]
31. Wang, R.; Zhang, J.; Wang, C.; Guo, E. Characteristic Analysis of Droughts and Waterlogging Events for Maize Based on a New Comprehensive Index through Coupling of Multisource Data in Midwestern Jilin Province, China. *Remote Sens.* **2020**, *12*, 60. [CrossRef]
32. Peng, C.; Deng, M.; Di, L.; Han, W. Delivery of agricultural drought information via web services. *Earth Sci. Inform.* **2015**, *8*, 527–538. [CrossRef]
33. Mo, K.C.; Lettenmaier, D.P. Objective Drought Classification Using Multiple Land Surface Models. *J. Hydrometeorol.* **2014**, *15*, 990–1010. [CrossRef]
34. Rajsekhar, D.; Singh, V.P.; Mishra, A.K. Multivariate drought index: An information theory based approach for integrated drought assessment. *J. Hydrol.* **2015**, *526*, 164–182. [CrossRef]
35. Qiu, R.; Li, X.; Han, G.; Xiao, J.; Ma, X.; Gong, W. Monitoring drought impacts on crop productivity of the U.S. Midwest with solar-induced fluorescence: GOSIF outperforms GOME-2 SIF and MODIS NDVI, EVI, and NIRv. *Agric. For. Meteorol.* **2022**, *323*, 109038. [CrossRef]
36. Li, X.; Xiao, J. A Global, 0.05-Degree Product of Solar-Induced Chlorophyll Fluorescence Derived from OCO-2, MODIS, and Reanalysis Data. *Remote Sens.* **2019**, *11*, 517. [CrossRef]
37. Meza, I.; Siebert, S.; Döll, P.; Kusche, J.; Herbert, C.; Rezaei, E.E.; Nouri, H.; Gerdener, H.; Popat, E.; Frischen, J.; et al. Global-scale drought risk assessment for agricultural systems. *Nat. Hazards Earth Syst. Sci.* **2020**, *20*, 695–712. [CrossRef]
38. Johnson, J.W. A Heuristic Method for Estimating the Relative Weight of Predictor Variables in Multiple Regression. *Multivar. Behav. Res.* **2000**, *35*, 1–19. [CrossRef] [PubMed]
39. Shi, W.; Wang, M.; Liu, Y. Crop yield and production responses to climate disasters in China. *Sci. Total. Environ.* **2021**, *750*, 141147. [CrossRef] [PubMed]
40. Zhao, H.; Xu, Z.; Zhao, J.; Huang, W. A drought rarity and evapotranspiration-based index as a suitable agricultural drought indicator. *Ecol. Indic.* **2017**, *82*, 530–538. [CrossRef]
41. Allen, R.G.; Pereira, L.S.; Raes, D.; Smith, M. *Crop Evapotranspiration-Guidelines for Computing Crop Water Requirements-FAO Irrigation and Drainage Paper 56*; FAO: Rome, Italy, 1998; Volume 300, p. D05109.
42. Paulo, A.; Rosa, R.D.; Pereira, L.S. Climate trends and behaviour of drought indices based on precipitation and evapotranspiration in Portugal. *Nat. Hazards Earth Syst. Sci.* **2012**, *12*, 1481–1491. [CrossRef]
43. Kogan, F. World droughts in the new millennium from AVHRR-based vegetation health indices. *Eos Trans. Am. Geophys. Union* **2002**, *83*, 557–563. [CrossRef]
44. Kogan, F.; Guo, W.; Yang, W. SNPP/VIIRS vegetation health to assess 500 California drought. *Geomat. Nat. Hazards Risk* **2017**, *8*, 1383–1395. [CrossRef]
45. Zhang, L.; Jiao, W.; Zhang, H.; Huang, C.; Tong, Q. Studying drought phenomena in the Continental United States in 2011 and 2012 using various drought indices. *Remote Sens. Environ.* **2017**, *190*, 96–106. [CrossRef]
46. Bhanja, S.N.; Mukherjee, A.; Saha, D.; Velicogna, I.; Famiglietti, J.S. Validation of GRACE based groundwater storage anomaly using in-situ groundwater level measurements in India. *J. Hydrol.* **2016**, *543*, 729–738. [CrossRef]

47. Feng, Y.; Liu, W.; Sun, F.; Wang, H. Changes of compound hot and dry extremes on different land surface conditions in China during 1957–2018. *Int. J. Climatol.* **2021**, *41*, E1085–E1099. [CrossRef]
48. Li, K.; Tong, Z.; Liu, X.; Zhang, J.; Tong, S. Quantitative assessment and driving force analysis of vegetation drought risk to climate change: Methodology and application in Northeast China. *Agric. For. Meteorol.* **2020**, *282–283*, 107865. [CrossRef]
49. Adarsh, S.; Reddy, M.J. Trend analysis of rainfall in four meteorological subdivisions of southern India using nonparametric methods and discrete wavelet transforms. *Int. J. Clim.* **2015**, *35*, 1107–1124. [CrossRef]
50. Du, C.; Chen, J.; Nie, T.; Dai, C. Spatial–temporal changes in meteorological and agricultural droughts in Northeast China: Change patterns, response relationships and causes. *Nat. Hazards* **2022**, *110*, 155–173. [CrossRef]
51. Xue, L.; Kappas, M.; Wyss, D.; Putzenlechner, B. Assessing the Drought Variability in Northeast China over Multiple Temporal and Spatial Scales. *Atmosphere* **2022**, *13*, 1506. [CrossRef]
52. Li, H.; Zhang, H.; Li, Q.; Zhao, J.; Guo, X.; Ying, H.; Deng, G.; Rihan, W.; Wang, S. Vegetation Productivity Dynamics in Response to Climate Change and Human Activities under Different Topography and Land Cover in Northeast China. *Remote Sens.* **2021**, *13*, 975. [CrossRef]
53. Zhao, Z.; Wang, K. Capability of Existing Drought Indices in Reflecting Agricultural Drought in China. *J. Geophys. Res. Biogeosci.* **2021**, *126*, e2020JG006064. [CrossRef]
54. Wu, B.; Ma, Z.; Yan, N. Agricultural drought mitigating indices derived from the changes in drought characteristics. *Remote Sens. Environ.* **2020**, *244*, 111813. [CrossRef]
55. Hu, Q.; Pan, F.; Pan, X.; Hu, L.; Wang, X.; Yang, P.; Wei, P.; Pan, Z. Dry-wet variations and cause analysis in Northeast China at multi-time scales. *Theor. Appl. Climatol.* **2018**, *133*, 775–786. [CrossRef]
56. Mao, D.; He, X.; Wang, Z.; Tian, Y.; Xiang, H.; Yu, H.; Man, W.; Jia, M.; Ren, C.; Zheng, H. Diverse policies leading to contrasting impacts on land cover and ecosystem services in Northeast China. *J. Clean. Prod.* **2019**, *240*, 117961. [CrossRef]
57. Hu, Y.; Zhou, B.; Han, T.; Li, H.; Wang, H. Out-of-Phase Decadal Change in Drought Over Northeast China Between Early Spring and Late Summer Around 2000 and Its Linkage to the Atlantic Sea Surface Temperature. *J. Geophys. Res. Atmos.* **2021**, *126*, e2020JD034048. [CrossRef]
58. Garba, I.; Salifou, I.; Sallah, A.; Samba, A.; Toure, I.; Yapo, Y.; Agoumo, A.; Soumana, S.; Oumarou, A.; Tychon, B.; et al. Mapping of zones at risk (ZAR) in West Africaby using NGI, VCI and SNDVI from the e-station. *Int. J. Adv. Res.* **2017**, *5*, 1377–1386. [CrossRef] [PubMed]
59. Liu, Z.; Hubbard, K.; Lin, X.; Yang, X. Negative effects of climate warming on maize yield are reversed by the changing of sowing date and cultivar selection in Northeast China. *Glob. Chang. Biol.* **2013**, *19*, 3481–3492. [CrossRef] [PubMed]
60. Yin, X.G.; Jabloun, M.; Olesen, J.E.; Öztürk, I.; Wang, M.; Chen, F. Effects of climatic factors, drought risk and irrigation requirement on maize yield in the Northeast Farming Region of China. *J. Agric. Sci.* **2016**, *154*, 1171–1189. [CrossRef]
61. Dai, M.; Huang, S.; Huang, Q.; Leng, G.; Guo, Y.; Wang, L.; Fang, W.; Li, P.; Zheng, X. Assessing agricultural drought risk and its dynamic evolution characteristics. *Agric. Water Manag.* **2020**, *231*, 106003. [CrossRef]